

# Nonlinear magneto-optical rotation narrowing in vacuum gas cells due to interference between atomic dark states of two spatially separated laser beams

M. M. Mijailović,<sup>\*</sup> Z. D. Grujić, M. Radonjić, D. Arsenović, and B. M. Jelenković  
*Institute of Physics, University of Belgrade, 11080 Belgrade, Serbia*

(Received 18 August 2009; published 12 November 2009)

We present, experimentally and theoretically, nonlinear magneto-optical rotation (NMOR) using two spatially separated laser beams, the pump laser beam for creation and the probe laser beam for detection of the coherence between ground Zeeman sublevels. Both pump and probe lasers are tuned to  $F_g=2 \rightarrow F_e=1$  transition in  $^{87}\text{Rb}$ . With the specially designed spatial configuration of the pump and the probe beams we were able to obtain dispersively shaped probe laser NMOR resonances in the Rb vacuum gas cell. The theory indicates that the obtained line shapes are due to the interference between prepared atomic states and the probe laser field. The interference nature of the resonances is supported by narrowing of NMOR resonances with increased separation between laser beams, and by the shift of the central fringe from the zero magnetic field with increased angle between initial orientation of electric vectors of linearly polarized pump and probe beams.

DOI: [10.1103/PhysRevA.80.053819](https://doi.org/10.1103/PhysRevA.80.053819)

PACS number(s): 42.50.Gy, 42.50.Nn, 42.65.-k

## I. INTRODUCTION

Nonlinear magneto-optical rotation (NMOR) of laser polarization is described with the three-stage interaction process: initial excitation of atomic ground-state coherence (here after coherence) and polarization, their evolution in the external magnetic field, and scattering of the laser field on the modified Zeeman coherence [1,2]. This theory was later extended by Budker *et al.* [3,4], by taking into account the alignment-to-orientation conversion process, which becomes dominant for a more powerful laser field. An alternative approach to the description of the NMOR of strong laser field polarization is based on the strong dependence of the refractive indices for two circularly polarized components of the electromagnetic field on the magnetic field in a coherent medium [5,6]. Both theoretical approaches provide good agreement with experimental results in thermal Rb vapor [6–9]. NMOR due to coherence effects is related to well-studied coherent population trapping (CPT) [10] and electromagnetically induced transparency (EIT) [11]. In CPT, and in NMOR due to coherences, the laser radiation prepares the atoms in a coherent superposition of states, one of which is nonabsorbing or dark state. This is typically achieved in  $\Lambda$  atomic scheme, when a ground-state doublet is coupled to a common excited state.

Narrow resonances of NMOR have important applications in magnetometry [12,13]. Recent developments of reliable and tunable laser diodes led to improvement in the sensitivity of magnetometers based on NMOR, surpassing (with  $10^{-15} \text{ THz}^{-1/2}$ ) superconducting quantum interference device magnetometers [14,15]. A simple device, based on alkali metal atoms vapor as a resonant medium, is capable of measuring extremely weak magnetic fields, like magnetic fields of the heart or the brain. Width of the NMOR resonance depends on the relaxation time of polarization and coherences. In vacuum gas cells the resonance width depends on the atom transit time through the laser light. In order to slow

atoms in the cell and increase interaction time with the light alkali metal gas cells with a buffer gas are used. Gas cells with paraffin coating on the walls are alternative method for narrowing NMOR resonances. Such coatings reduce relaxation of atom polarization and allow coherently prepared atom to bounce many times between walls, and increase its interaction time with the laser light [12,16]. When residual (stray) magnetic fields are negligible, ultra narrow NMOR resonances of 1 Hz are obtained [12,17].

Narrowing of EIT resonances due to repeated interaction of the laser light with the atom was studied in both buffer-gas cells and in cells with the wall coating. In buffer-gas cells collisions between Rb atom and the buffer gas due to extremely low spin-exchange cross section do not destroy the quantum coherence, but prolong the time that atom stays inside the laser beams. At the same time, collisions with the buffer gas can send a fraction of Rb atom back to the laser beam. When coherence is transferred out and back again into the excitation region, the narrowing is due to two-photon Raman-Ramsey interference effect [18,19]. In vapor cells with antirelaxation wall coating these effects are due to multiple bouncing of the atomic coherence from the cell walls [20]. The narrow EIT resonances, analogous to Ramsey fringes, were also observed in the pump-probe laser configuration, in atomic cells filled with inert buffer gas due to spatially [21] and temporarily separated probe and pump [22]. Ramsey fringes were also observed in the NMOR spectroscopy, in thermal Rb atomic beam with spatially separated pumping and probing regions [23].

Most of experimental and theoretical studies of Raman-Ramsey effects were done using buffered gas cells. There are a few disadvantages of using buffer-gas cells for important applications of CPT and NMOR. Collisions with the buffer gas cause a temperature sensitive frequency shift, proportional to the buffer-gas pressure in a sealed cell. In the medium with collisional broadening the effect of velocity changing collisions on Zeeman coherence can be very large. The atoms that are returned to the excitation region have different direction and magnitude of the velocity that results in mixing Zeeman orthogonal dark states formed on different

<sup>\*</sup>marina.mijailovic@phy.bg.ac.rs

$\Lambda$  schemes [24,25]. It is often desired to have gas cells at higher temperatures since increased density of atoms improves sensitivity of magnetometers [14]. Increase in the atom density in buffered gas cells is limited to values below which the collision relaxation becomes dominant mechanism. There are only few studies of Raman-Ramsey effects in vacuum gas cells, and they are related mainly to EIT. Repeated interactions of atom with the laser fields, mutually parallel and spatially separated by a few millimeters, produce highly visible Ramsey fringes in the buffer-gas cell, but almost invisible fringes in the vacuum cell [21]. On the other hand, considerable narrowing of the probe EIT in Rb vacuum cell due to the Ramsey effect was observed when spatially separated pump beam completely surrounds the probe beam [26].

In this paper we present an observation of effects of Ramsey type interference on NMOR resonances in the vacuum gas cell at room temperature, using the same beam configuration as in [26]. In the experiment, Zeeman  $\Delta m=2$  coherence between sublevels of the  $F=2$  hyperfine level of  $^{87}\text{Rb}$  in  $D_1$  line was carried by atomic thermal motion from the coaxial hollow pump beam to the probe beam. Rotation of the linear probe polarization, as a function of the external magnetic field, for different angles between electric vectors of the pump and probe beams is measured using balanced polarimeter. Obtained dispersive like line shapes with the first-order Ramsey fringes are compared with calculated NMOR resonances. Time-dependent optical Bloch equations were used to calculate density-matrix elements for atoms in the Rb vapor. All the levels interacting with the laser light are taken into account, as well as population losses to the another ground-state hyperfine level. Rotation of the probe beam polarization is obtained from calculated changes of the probe electric field due to Rb vapor polarization, averaged over atom velocity distribution.

## II. THEORY

We used density-matrix formalism to analyze the dynamics of the interaction between Rb atoms and spatially separated pump and probe laser beams. Figure 1(a) shows Rb atomic level diagrams with Zeeman sublevels coupled by the laser light. The external magnetic field  $B$ , along the laser beam propagation, splits the Zeeman sublevels by the amount  $\mu_B g_F B$ , where  $\mu_B$  is the Bohr magneton and  $g_F$  is the gyromagnetic factor of the level. The temporal evolution of the density-matrix elements for the excited and the ground-state populations and coherences ( $\rho_{e_i e_j}, \rho_{g_i g_j}$ ), and for optical coherence ( $\rho_{e_i g_j}$ ) is obtained from time-dependent optical Bloch equations for the open  $F_g=2 \rightarrow F_e=1$  transition in  $^{87}\text{Rb}$  [26].

Both the pump and the probe beams have the same frequency  $\omega$  and propagate along the  $z$  axis. As schematically given in Fig. 1(b), the probe laser beam is at the center of the hollow pump beam. Pump beam intensity profile along radial distance  $r$  is modeled by

$$\frac{\text{Erf}((r-r_1)/a(r_2-r_1)) - \text{Erf}((r-r_2)/a(r_2-r_1))}{2},$$

where  $r_1$ ,  $r_2$ , and  $a$  are suitable parameters. The radial probe beam profile is a Gaussian.

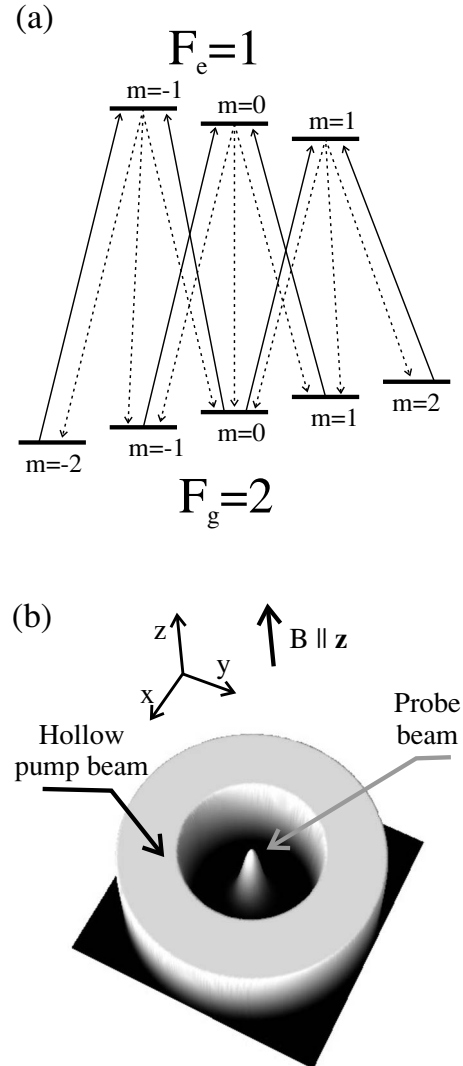


FIG. 1. (a) The energy-level diagram for magnetic sublevels of the  $F_g=2 \rightarrow F_e=1$  transition where solid line represent laser light coupling Zeeman sublevels and dotted lines show the de-excitation paths from excited levels. (b) Schematic of spatial configuration of the pump and the probe laser beam radial profiles used in the theoretical model.

We assume that each collision with the wall resets the state of an atom. Therefore, atoms entering the pump beam from the direction of the wall have equally populated Zeeman sublevels of both ground-state hyperfine levels. Numerical integration of the optical Bloch equations is carried out from the moment when the atom enters the pump beam region until it exits the probe beam region. The density of the rubidium vapor is low enough, so we can ignore relaxation of coherence due to Rb-Rb collisions.

Populations of the excited levels and absorption of the probe laser light were studied in our previous work [26]. In this work, we calculate angle of rotation of the linearly polarized probe laser light as a function of magnetic field. The effects of the laser propagation and variation in its intensity along the Rb cell are included in the following manner. First, we calculate the Rb vapor polarization assuming constant electric field along the  $z$  direction within the cell and after-

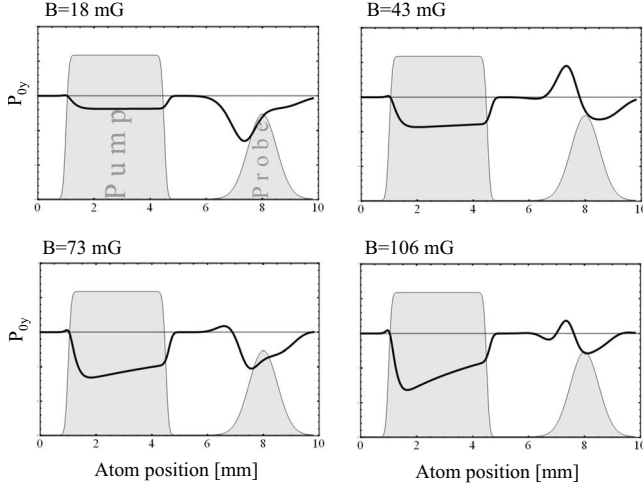


FIG. 2. Calculated dependence of the  $y$  component of the  $\vec{P}_0$  as a function of the radial position of the atom passing through the pump beam, the dark region and the probe region. The shaded area shows the radial position and the intensity profile of the pump and the probe beam at a different scale. Results are given for the magnetic field values of 18, 43, 73, and 106 mG, respectively, and pump and probe powers of 1.2 mW and 10  $\mu$ W. Polarizations of the pump and probe beam are linear and mutually parallel. Atom passes perpendicularly to the laser beam, with velocity of 260 m/s. The inner pump beam diameter is 7 mm and the probe beam  $1/e^2$  width is 1.2 mm.

wards obtain the change in the electric field using the calculated polarization. Polarization of Rb vapor in the laser light is obtained using

$$\begin{aligned} \vec{P} &= ne\text{Tr}[\hat{\rho} \cdot \hat{r}] = n\vec{P}_0 e^{-i\omega t} + c.c., \\ \vec{P}_0 &= \sum_i \sum_j \rho_{e_i g_j} \left[ \frac{\mu_{g_f e_i-1} - \mu_{g_f e_i 1}}{\sqrt{2}} \vec{e}_x \right. \\ &\quad \left. + i \frac{\mu_{g_f e_i-1} + \mu_{g_f e_i 1}}{\sqrt{2}} \vec{e}_y + \mu_{g_f e_i 0} \vec{e}_z \right], \end{aligned} \quad (1)$$

where  $n$  is the vapor concentration. During propagation of the probe laser through the optically thin Rb vapor, the electric field changes according to

$$\frac{\partial \vec{E}}{\partial z} = \frac{1}{2} ik \frac{n\vec{P}_0}{\epsilon_0}. \quad (2)$$

The assumption  $|\Delta \vec{E}| \ll |\vec{E}|$  leads to

$$\frac{\partial \vec{E}}{\partial z} \approx \frac{\Delta \vec{E}}{\Delta z} \Rightarrow \Delta \vec{E}(r) = \frac{1}{2} ik \frac{n\vec{P}_0(r)}{\epsilon_0} L, \quad (3)$$

where  $k = \omega/c$ ,  $L$  is cell length, and  $\epsilon_0$  is the dielectric constant.

Figure 2 shows the changes of the  $y$  component of the atomic polarization  $\vec{P}_0$ , as a function of the atom radial position. Assuming that the initial polarizations of the pump and probe beam are linear and in the direction of the  $x$  axis,  $y$  component of  $\vec{P}_0$  is proportional to the angle of the probe

beam polarization rotation induced by the atom. Results are given for several representative values of the magnetic field. As schematically indicated by the shaded areas, the atom enters and crosses the pump region, traverses the region between the laser fields, and then enters the probe beam region. Results in Fig. 2 are for atom moving perpendicularly to the laser beam at the velocity of  $v = 260$  m/s, which is the mean atomic velocity of Rb atoms in room-temperature cell. The behavior of atomic polarization in the probe beam depends on the phase of the atomic state when atom enters the probe. This phase is determined by the magnetic field and the atomic velocity. The intensity of the probe laser light further determines the behavior of atomic polarization in the probe beam. As seen in Fig. 2 the atomic polarization can have different signs, meaning that atom will induce rotation of the probe laser beam polarization in different directions. The total effect of an atom in Fig. 2 on the probe beam polarization rotation is obtained by integration along the probe beam.

The probe laser beam electric vector, after the laser passes the Rb cell, is calculated from

$$\vec{E}_{out}(r) = \vec{E}(r) + \langle \Delta \vec{E}(r, \vec{v}) \rangle_{\vec{v}}, \quad (4)$$

where  $\vec{E}(r)$  is the electric field at the entrance in the cell and  $\Delta \vec{E}(r, \vec{v})$  is the change in electric field due to single velocity class  $\vec{v}$  given by Eq. (3). The average  $\langle \cdot \rangle_{\vec{v}}$  in Eq. (4) is over the Maxwell-Boltzmann velocity distribution  $W_b$ ,

$$\langle \Delta \vec{E}(r, \vec{v}) \rangle_{\vec{v}} = \int_{\vec{v}} W_b(T, |\vec{v}|) \Delta \vec{E}(r, \vec{v}) d\vec{v}, \quad (5)$$

where

$$W_b(T, v) = 4\pi \left( \frac{m}{2\pi kT} \right)^{3/2} v^2 e^{-mv^2/2kT}. \quad (6)$$

Here,  $m$  is the atom mass,  $k$  is Boltzmann constant, and  $T$  is the absolute temperature.

The angle  $\varphi$  of the polarization rotation is calculated in the similar manner as experimentally measured, from signals of the two detectors  $S_1$  and  $S_2$  behind the polarizing beam splitter, rotated at  $45^\circ$  in respect to the incident polarization (see Fig. 3). Polarization rotation is given by

$$\varphi = \frac{1}{2} \arcsin \frac{S_1 - S_2}{S_1 + S_2}. \quad (7)$$

Values of  $S_1$  and  $S_2$  were obtained from

$$S_{1,2} = \frac{c\epsilon_0}{2} \int_{d_p} |\vec{u}_{1,2} \cdot \vec{E}_{out}(r)|^2 dr, \quad (8)$$

where  $\vec{u}_{1,2} = (\sqrt{2}/2)(\vec{e}_x \pm \vec{e}_y)$  are unity vectors corresponding to polarizing beam splitter's  $s$  and  $p$  polarization axes and  $d_p$  is the probe beam diameter. Numerical computation in Eqs. (5) and (8) is done by substituting the integration by the summation. During the calculations of the probe polarization rotation we assumed that the pump beam polarization remains oriented along the  $x$  axis.

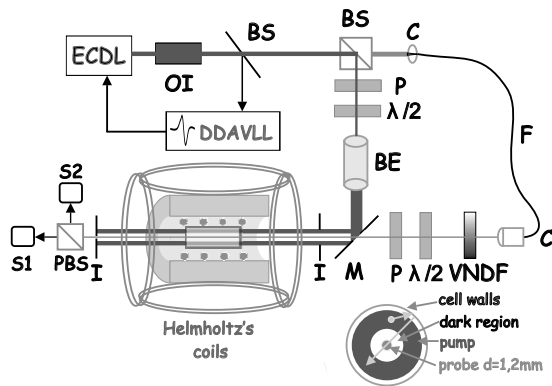


FIG. 3. Experimental setup: ECDL-external cavity diode laser, OI-optical isolator, DDAVLL-Doppler-free dichroic atomic laser lock, BS-beam splitter, C-collimator, F-fiber, I-iris, P-polarizer, VNDF-variable neutral density filter, BE-beam expander, M-mirror,  $\lambda/2$ -retardation plates, PBS-polarizing beam splitter,  $S_1$ ,  $S_2$ -signals from photodiodes.

### III. EXPERIMENTAL SETUP

The experiment is schematically shown in Fig. 3. The laser light is generated by the external cavity diode laser and locked to the  $D_1$  transition in  $^{87}\text{Rb}$  using Doppler-free dichroic atomic vapor laser lock (DDAVLL) technique [27]. The laser beam is divided into two beams using nonpolarizing beam splitter. The intensities of the two beams are adjusted by variable neutral density filters. The diameter of one of the beams (the pump beam) is enlarged to  $\sim 25$  mm and sent through the 12 mm diameter iris. The linear polarization of the pump beam and its orientation in respect to the linear polarization of the probe beam are adjusted by a linear polarizer and  $\lambda/2$  retardation plate. The polarization of the probe beam is regulated by the linear polarizer. The two beams are combined using 25 mm diameter mirror with the hole in its center [28]. Thus, the diameter of the hole determines the inner diameter of the pump beam. The probe beam, 1.2 mm in diameter, passes through the center of the hole. Both beams pass through the Rb cell with length of 85 mm and diameter of 25 mm.

In order to minimize stray magnetic fields, the Rb cell is placed in the center of three pairs of Helmholtz coils arranged on the cubic frame. A hollow aluminum cylinder (40 cm length, internal diameter 6 cm, thickness 4.5 cm) is used for shielding against ac stray magnetic fields. Measured residual inhomogeneity of the total magnetic field was less than 5 mG over the cell's length. Scanning magnetic field  $B$ , in the direction of the laser beams propagation, is generated by the solenoid around the gas cell.

Behind the cell, the probe beam passes through the iris which is slightly larger than the probe beam diameter, in order to minimize the pump beam contribution to the measured probe laser transmission. The probe beam then passes through the polarization beam splitter with the fast axis oriented at  $45^\circ$  in respect to the direction of the initial polarization of the probe beam. Two beams emerging from the polarizing beam splitter were detected with two photodiodes. The sum ( $S_1 + S_2$ ) and the difference ( $S_1 - S_2$ ) of signals of the

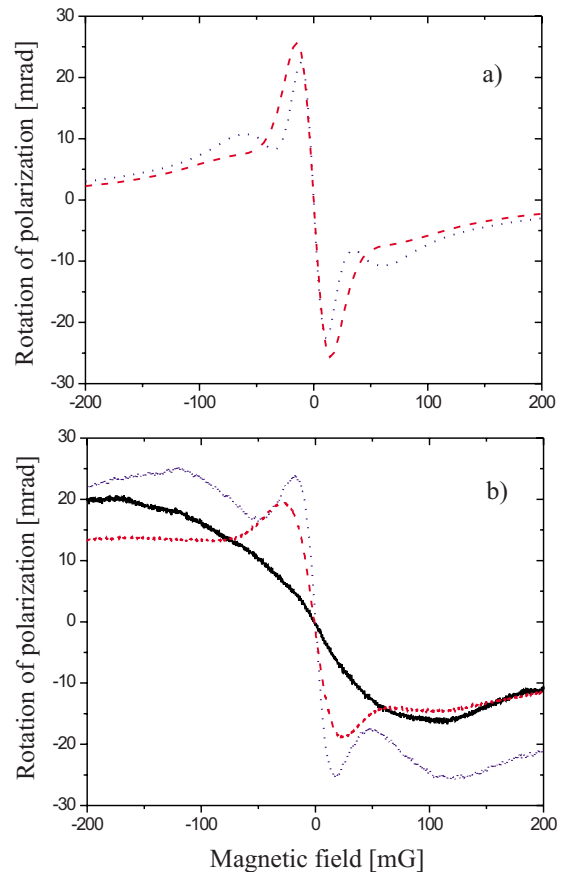


FIG. 4. (Color online) Calculated (a) and measured (b) angle of the polarization rotation of the linear probe polarization as a function of the axial magnetic field. Dashed and dotted lines are for two inner pump beam diameters 5 mm and 7 mm, respectively. The solid line in (b) is the probe beam polarization rotation angle when the pump beam is turned off. The pump and the probe beams have parallel linear polarization and are tuned to the  $F_g=2 \rightarrow F_e=1$  transition in  $^{87}\text{Rb}$ . The probe and the pump laser powers are  $10 \mu\text{W}$  and 1.2 mW, respectively.

two detectors were recorded by the digital oscilloscope, while  $B$  was scanned around its zero value. In this configuration the polarization rotation angle  $\varphi$  is given by the Eq. (7).

### IV. RESULTS AND DISCUSSION

In the following, we show the probe NMOR resonances, i.e., the angle of rotation of the linear probe polarization as a function of the external magnetic field  $B$ . In the experiment, the magnetic field varies slowly (50 Hz) so that the period of a magnetic sweep is much longer than the atom transit time. This justifies the assumption made in the model that the magnetic field  $B$  is constant, while atom passes through the three regions (the pump beam region, the dark region and the probe region). For all presented results, spatially displaced pump and probe beams have the same frequency.

Figures 4(a) and 4(b) present calculated and measured angle of rotation of the linear probe polarization as a function of the axial magnetic field. The polarizations of the

pump and the probe beams are linear and parallel. When the pump laser is turned on, the probe NMOR resonance has a narrow central dispersive fringe and weak sidebands. As shown in the Fig. 4(b), substantial change in the NMOR wave form occurs when the pump beam is turned off. When the pump beam is turned on, the width of the central NMOR peak is narrower than the one obtained using single laser beam with the beam diameter as large as the gas cell diameter. Results are given for two inner pump beam diameters, 5 mm and 7 mm. Resonance width decreases when a distance between the pump and the probe increases, which is a characteristic of Ramsey interference.

The Zeeman  $\Delta m = \pm 2$  coherence in the  $F_g = 2$  hyperfine level induced by the pump beam oscillates in the magnetic field at the Larmor frequency. The phase of the coherence when atom enters the probe region depends on this frequency and the time of flight through the dark region. The interaction with the probe laser, in a phase with the pump laser field, causes the interference with the atomic coherence carried by the moving atom. The probe beam polarization rotation reflects this interference by the appearance of line shapes with Ramsey fringes. The observed wave forms are results of contributions of atomic coherence and of the probe beam itself [see for example solid curve in Fig. 4(b)]. Due to the thermal distribution of atom velocities, only first-order fringes of low contrast are present. At the low probe laser power, the probe contribution does not overwhelm the effect of atomic coherence. As we will show later, when the probe power exceeds certain threshold, single beamlike NMOR is obtained. Results given in Figs. 4(a) and 4(b) show very good agreement between theoretical predictions and experimental measurements.

The role of the interference is evident from observed dependence of NMOR wave forms on the phase difference between the probe beam and the atomic coherence. Controllable phase difference was induced by varying the initial angle between the pump and the probe beam polarization. In Fig. 5, we present the results for the probe beam polarization rotation for several angles between the electric vectors of linearly polarized pump and probe beams. The atomic coherence created by the linearly polarized pump beam is proportional to  $\vec{E}_p^+ \cdot \vec{E}_p^-$ , where  $\vec{E}_p^{+(-)}$  are circular  $\sigma^{+(-)}$  components of linearly polarized radiation [5,22]. Rotating the polarization of the pump beam by the angle  $\varphi$ , the phase between the circular components of the pump beam is changed by  $2\varphi$ . This causes changes of the relative phase of the coherence with respect to the probe (all other parameters being the same). Setting the angle between the two electric field vectors to  $\pi/2$ , we obtained the opposite sign for the probe beam polarization rotation. For the angle  $\varphi$  between 0 and  $\pi/2$  the dispersionlike curves for the probe NMOR beam are centered at external magnetic field different from zero. The magnetic field corresponding to the center of the NMOR resonance increases with the angle between polarizations of two beams because different phases of the coherence require different magnetic field (i.e., Larmor frequency) for the constructive interference to occur. The amplitude of the central peak decreases as the angle  $\varphi$  and consequently the magnetic field related to the center of NMOR are increasing. This is due to the fact that at higher magnetic fields the populations

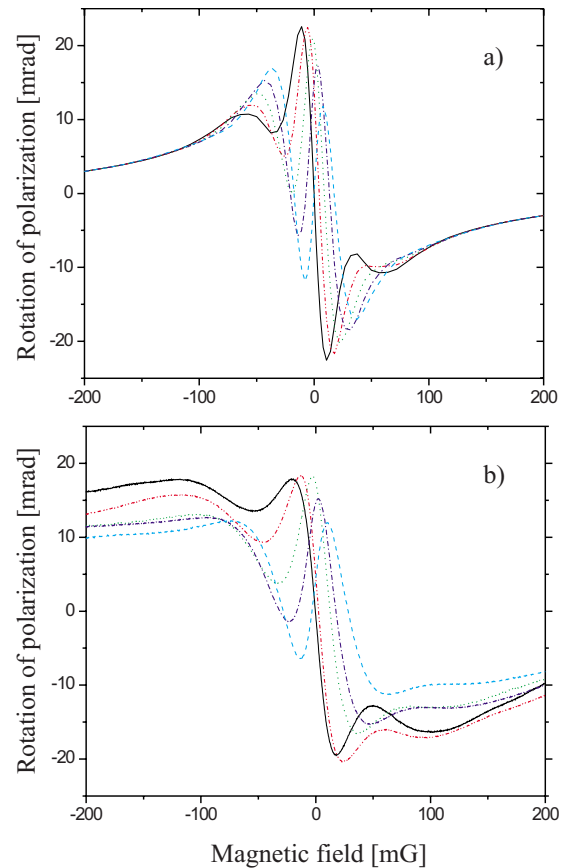


FIG. 5. (Color online) Theoretical (a) and experimental (b) results for the angle of rotation of the probe polarization for different angles between linear polarization of the pump and the probe ( $0^\circ$  solid,  $22.5^\circ$  dash-dot-dot,  $45^\circ$  dotted,  $67.5^\circ$  dash-dot and  $90^\circ$  dashed lines). The pump and the probe beams are tuned to the  $F_g = 2 \rightarrow F_g = 1$  transition in  $^{87}\text{Rb}$ . The probe and the pump laser powers are  $10 \mu\text{W}$  and  $1.2 \text{ mW}$ , respectively. The pump beam inner diameter is  $7 \text{ mm}$ .

and coherences of Zeeman ground sublevels are lower, because of enhanced pumping into the uncoupled  $F_g = 1$  hyperfine level. The comparison between results in Figs. 5(a) and 5(b) shows that calculated and measured line shapes are very similar.

The effects of the probe laser power on the probe polarization rotation are given in Fig. 6. Both theory and experiment, show that an increase in the probe beam power lowers the amplitudes of the narrow central NMOR resonance. Higher probe beam power increases the probe beam contribution and simultaneously lowers the effects of the pump beam induced atomic coherence. Note that as long as the effect of atomic coherence entering the probe beam is not negligible, the resonance width of the central peak remains the same. Beyond the probe beam power of  $200 \mu\text{W}$ , NMOR resonance is predominantly determined by the probe laser excitation and, like in the case of the single laser beam has wave form with strongly attenuated interference features [see solid curve in Fig. 4(b)].

The dispersion like structure presented in Figs. 4 and 5 has linewidth of the order of  $30 \text{ mG}$ . This is nearly five times narrower than the linewidth determined by the transit time of

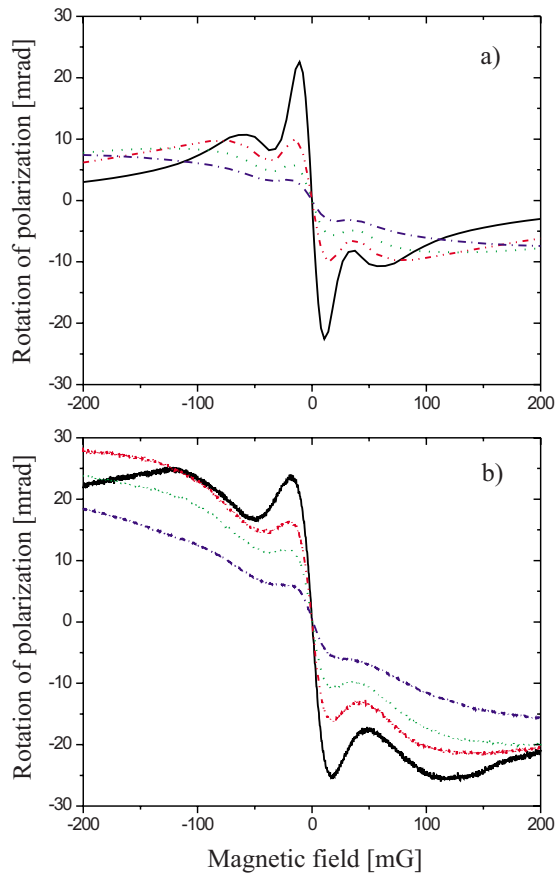


FIG. 6. (Color online) Theoretical (a) and experimental (b) results for the rotation of the probe polarization spectra for different powers of the probe beam (10  $\mu\text{W}$  solid, 50  $\mu\text{W}$  dash-dot-dot, 100  $\mu\text{W}$  dotted, 200  $\mu\text{W}$  dash-dot). The pump and the probe beams are tuned to the  $F_g=2 \rightarrow F_e=1$  transition in  $^{87}\text{Rb}$  and have parallel linear polarization. The pump laser power is 1.2 mW. The inner pump beam diameter is 7 mm.

the atom through the probe laser beam [Fig. 4(b)]. But typical linewidths of resonances in our experiment are much wider than resonances obtained with the single laser beam in a vapor cell with antireflection coating [12]. The resonance

width obtained in our experiment will be narrower if better shielding of the cell from stray magnetic fields is provided. Nevertheless, narrow resonances as in [12] can only be obtained with cells with well made coating that preserves atomic coherence and alignment over thousands of wall collisions.

## V. CONCLUSION

We have studied experimentally and theoretically the probe polarization NMOR for the  $D_1$  line transition  $F_g=2 \rightarrow F_e=1$  in  $^{87}\text{Rb}$  in the presence of spatially separated pump laser beam. Our configuration of spatially separated hollow pump and coaxial probe beam provides sufficient flux of coherently prepared atoms in the probe beam enabling the observation of theoretically predicted narrow Ramsey fringes in the probe NMOR in vacuum cells. The shape of the probe NMOR at different spacing between pump and probe beams, and for different orientation of the polarization of the pump and the probe beam is explained through interference between the pump prepared atomic coherence and the probe laser field. Our realization extends previous approaches in enhancing sensitivity to Ramsey effects in buffered gas cells and cells with coated walls, to vacuum gas cells. When compared to the single laser beam Hanle configuration setup, we obtained substantial NMOR narrowing due to interference effects. Although this is still much wider than resonances obtained with cells with antireflection coating, further resonance narrowing in our setup is possible by increasing the distance between the pump and the probe beam and by using better shielding of the gas cell from stray magnetic fields. Narrow resonances obtained using vacuum gas cells are not affected by the frequency shifts due to wall collisions and may have important role in precision spectroscopy and magnetometry.

## ACKNOWLEDGMENTS

This work was supported by the Ministry of Science and Technological Development Republic of Serbia, under Grant No. 141003.

- 
- [1] A. Weis, J. Wurster, and S. I. Kanorsky, *J. Opt. Soc. Am. B* **10**, 716 (1993).  
 [2] S. I. Kanorsky, A. Weis, J. Wurster, and T. W. Hänsch, *Phys. Rev. A* **47**, 1220 (1993).  
 [3] D. Budker, D. F. Kimball, S. M. Rochester, and V. V. Yashchuk, *Phys. Rev. Lett.* **85**, 2088 (2000).  
 [4] D. Budker, W. Gawlik, D. F. Kimball, S. M. Rochester, V. V. Yashchuk, and A. Weis, *Rev. Mod. Phys.* **74**, 1153 (2002).  
 [5] M. Fleischhauer, A. B. Matsko, and M. O. Scully, *Phys. Rev. A* **62**, 013808 (2000).  
 [6] V. A. Sautenkov, M. D. Lukin, C. J. Bednar, I. Novikova, E. Mikhailov, M. Fleischhauer, V. L. Velichansky, G. R. Welch, and M. O. Scully, *Phys. Rev. A* **62**, 023810 (2000).  
 [7] I. Novikova, A. B. Matsko, and G. R. Welch, *Opt. Lett.* **26**, 1016 (2001).  
 [8] S. M. Rochester and D. Budker, *J. Mod. Opt.* **49**, 2543 (2002).  
 [9] R. A. Akhmedzhanov and I. V. Zelensky, *JETP Lett.* **76**, 419 (2002).  
 [10] E. Arimondo, in *Progress in Optics*, edited by E. Wolf (Elsevier Science, Amsterdam, 1996), Vol. XXXV, Chap. V, pp. 259–354.  
 [11] S. E. Harris, *Phys. Today* **50**(7), 36 (1997).  
 [12] D. Budker, V. Yashchuk, and M. Zolotarev, *Phys. Rev. Lett.* **81**, 5788 (1998).  
 [13] V. Yashchuk, D. Budker, and M. Zolotarev, in *Trapped Charged Particles and Fundamental Physics*, edited by D. H. E. Dubin and D. Schneider (American Institute of Physics, New York, 1999).

- [14] D. Budker and M. V. Romalis, *Nat. Phys.* **3**, 227 (2007).
- [15] I. K. Kominis, T. W. Kornack, J. C. Allred, and M. V. Romalis, *Nature (London)* **422**, 596 (2003).
- [16] D. Budker, D. J. Orlando, and V. Yashchuk, *Am. J. Phys.* **67**, 584 (1999).
- [17] D. Budker, D. F. Kimball, S. M. Rochester, V. V. Yashchuk, and M. Zolotarev, *Phys. Rev. A* **62**, 043403 (2000).
- [18] I. Novikova, Y. Xiao, D. F. Phillips, and R. L. Walsworth, *J. Mod. Opt.* **52**, 2381 (2005).
- [19] Y. Xiao, I. Novikova, D. F. Phillips, and R. L. Walsworth, *Phys. Rev. Lett.* **96**, 043601 (2006).
- [20] S. I. Kanorsky, A. Weis, and J. Skalla, *Appl. Phys. B: Lasers Opt.* **60**, S165 (1995).
- [21] A. S. Zibrov and A. B. Matsko, *Phys. Rev. A* **65**, 013814 (2001).
- [22] A. S. Zibrov, I. Novikova, and A. B. Matsko, *Opt. Lett.* **26**, 1311 (2001).
- [23] B. Schuh, S. I. Kanorsky, A. Weis, and T. W. Hänsch, *Opt. Commun.* **100**, 451 (1993).
- [24] I. Novikova, A. B. Matsko, and G. R. Welch, *J. Opt. Soc. Am. B* **22**, 44 (2005).
- [25] E. E. Mikhailov, I. Novikova, Y. V. Rostovtsev, and G. R. Welch, *Phys. Rev. A* **70**, 033806 (2004).
- [26] Z. D. Grujić, M. Mijailović, D. Arsenović, A. Kovačević, M. Nikolić, and B. M. Jelenković, *Phys. Rev. A* **78**, 063816 (2008).
- [27] K. L. Corwin, Z. T. Lu, C. F. Hand, R. J. Epstein, and C. E. Wieman, *Appl. Opt.* **37**, 3295 (1998).
- [28] Chang Chun Bo Xin Photoelectric Co., Ltd., Chang Chun, Ji Lin, China, <http://www.bxoptic.com/>